Discover Materials

Research

Structural, chemical, and mechanical properties of concrete developed from a binder composite of sugarcane bagasse ash and Portland cement

Michael Evans Nzugua[1,3] · **Emma Panzi Mukhokosi**[1,4] · **Sam Obwoya Kinyera**[1,2]

Received: 27 September 2024 / Accepted: 4 March 2025
Published online: 05 June 2025

Abstract
The East Africa Community (EAC) countries have immense sugarcane cane bagasse ash (SCBA) which remains unexploited as a supplementary-cementitious material (SCM). This study delved into using EAC SCBA as a pozzolan. SCBA investigated was collected from Kenya's coastal area. Raw SCBA, processed SCBA, Portland cement (PC) and the developed concrete were characterised by various techniques to determine the surface morphology, chemical composition, structural properties and mineralogical composition. The raw SCBA was calcined at 600 °C then used to design the concrete mix. PC was replaced with SCBA from 0 to 30% in steps of 10%. The flexural and compressive strengths were determined in the hardened state after 28 days of concrete curing. The compressive and flexural strengths of the mix containing 20% SCBA were higher than the control mix by 9.65 and 6.51%, respectively. The microstructural properties of the developed concrete revealed dense particle distribution, indicating good micro/nanofiller effects of the interfacial transition zone (ITZ). The processed SCBA was found to meet class N and F of natural pozzolan as per ASTM C 618. This study suggests that the Kenya coastal SCBA can be used as a supplementary cementitious material.

Keywords Sugarcane bagasse ash · SEM · XRD · Supplementary cementitious materials · Pozzolans · Sustainable concrete

1 Introduction

Concrete, a combination of PC, water and aggregates is a widely used construction material due to the availability of raw materials, durability, good mechanical properties in the hardened state and the ease of moulding into various shapes [1–3]. PC is manufactured in a controlled chemical combination of silica, lime, alumina, sulphides, sodium carbonate, and iron [4]. Producing 1 ton of PC produces 1 ton of carbon dioxide (CO_2) [5], which increases the greenhouse gases (GHGs) and accelerates global warming. The average CO_2 equivalent produced in Mega tone per annum (Mt/a) of cement by major cement-producing countries globally ranges between 5.2 and 1170.10 Mt/a [6, 7]. This has contributed to the loss of biodiversity and an increase in the emission of GHGs. The need for affordable and sustainable concrete has given rise to using supplementary-cementitious materials (SCMs). SCMs, fly ash, lithium slag, granulated blast furnace slag, limestone

✉ Emma Panzi Mukhokosi, panzi2018@gmail.com; epmukhokosi@kyu.ac.ug | [1]Physics Department, Kyambogo University, P.O. Box 1, Kyambogo, Kampala, Uganda. [2]National Planning Authority, P.O. Box 21434, Kampala, Uganda. [3]Materials Testing and Research Division, Ministry of Roads and Transport, P.O. Box 11873, Nairobi, Kenya. [4]School of Natural and Applied Sciences, Kampala International University, P.O. Box 2000, Kampala, Uganda.

calcined clay cement (LC3), and SCBA among others have been studied by several researchers in different countries for their mechanical properties [8–13].

Several studies have examined the impact of SCBA on the mechanical properties of concrete, including compressive and flexural strength. For instance, Kannur and Chore [8], working on the strength and durability study of low-fines self-consolidating concrete using sugarcane bagasse ash, observed that SCBA increases the compressive strength up to a dosage of 20% above which the strength began to reduce. Bersisa and Zekaria [14], working on the assessment of mechanical properties of SCBA concrete determined that SCBA reduces early-age mechanical performance. Furthermore, the concrete containing SCBA dosages of 6.50% and 13.0% exceeded those of the control mix by 3.46% and 6.64% respectively on compressive strength. The maximum strength gain was realized at 13% of the SCBA dose with 20% dosage reducing the strength significantly. Similarly, Girma and Asteray [15] conducting research, on high-strength concrete made from SCBA concluded that SCBA dosages increase compressive strength at an early age of curing with maximum strength achieved at 10% after 28 days of curing. These observations contrasted those of Bersisa and Zekaria [14]. Correspondingly, Tarekegn et al. [16], researching on blended SCBA concrete observed optimised compressive strength at 10% SCBA dose. Similarly, Abdalla et al. [1] working on a blend of SCBA and silica fumes concrete properties, realized a significant increase in compressive strength at lower SCBA dosages with a decrease at higher doses. The optimum compressive strength above 60 MPa was observed at day twenty-eight with 10% SCBA inclusion.

For the flexural strength property on 28-days curing, Rebari et al. [17] showed that the addition of SCBA consistently decreased the concrete strength at all SCBA dosages. This was in great contrast with some researchers. Firstly, Praveenkumar and Sankarasubramanian [18] working on the mechanical and durability properties of bagasse ash blended concrete, observed that strength increased gradually from 2.09 to 3.08% for SCBA dosage of 5 and 10% respectively with optimized strength at 10%. Secondly, Bersisa and Zekaria [14] while assessing the mechanical properties of the bagasse ash concrete, reported that the early day's strength increased significantly for 6.5 and 13% SCBA dosage by 6.38 and 17% respectively. Finally Abdalla et al. [1] searching on eco-friendly concrete made with SCBA, noted that, 10% SCBA showed the highest strength of 8% above which the strength began to drop significantly.

In addition to the variations in strength caused by incorporating SCBA in concrete, the mineral composition of SCBA itself also varies. This was observed from different literature reviewed. The range of variations of the major mineral constituents are; silicon dioxide (30.27–77.25%), aluminium oxide (1.68–24.80%), iron oxide (0.90–15.0%), calcium oxide (1.69–10.07%), magnesium oxide (0.00–2.61%), manganese oxide (0.00–0.69%), and di-phosphorus trioxide (0.00–2.83%) [5, 19–21].

The literature reviewed showed that the optimum SCBA concrete mechanical properties (compressive and flexural strength) are realized at various SCBA dosages of 10, 13, and 20% aided by the myriads variations in minerals composition [8, 14, 15]. Most SCBA concrete had optimised strength at 10% cement replacement. It is interesting to note that these variations in the SCBA mineral composition depend on various factors, among them, the geographical location, type of sugarcane crop, underground water and soil type [5, 19].

In East Africa, SCMs like natural kamafugites, carbonatites, and diatomite are easy to find [22]. However, their efficiency and effectiveness for use as SCMs are not always reliable. Kamafugites rocks lack the needed reactive silica and alumina content so do carbonatites, while diatomite requires significant processing at very high temperatures to activate their inert silica for pozzolanic properties [23]. Their limitations in strength contribution, workability, and economic viability make them less suitable as natural semi-cementitious materials. Cement manufacturing companies have therefore resorted to artificial SCMs like granulated blast furnace slag and fly ash [24–27] which are not sustainable and their production contributes to GHGs. This has led to a growing search for alternative, locally available, and eco-friendly supplementary cementitious materials (SCMs) [28, 29]. The SCMs under consideration among the East African countries are majorly agricultural by-products rich in silica such as SCBA which are dumped in landfills where they stain air quality [17, 30, 31].

This paper is organised as follows: introduction, the significance of the study, materials and methods, results and discussions, conclusion and areas of recommendation for further studies.

1.1 Significance of the present investigation

For the first time, we investigate the Kenya coastal SCBA as a supplementary-cementitious material by examining the structural, elemental/chemical composition and mineralogical composition. We make concrete blocks and investigate the mechanical properties using a binder composite of SCBA and PC. This is done with the view of utilising SCBA in concrete production leading to a sustainable PC production chain (e.g. reduction of CO_2 in PC production, reduction in raw

mineral excavation), concrete affordability and mitigating the negative effects of SCBA waste disposal (creating circular economy) aligning with sustainable developments goals, 11, 12, and 13. This study adds to the body of literature on the use of the coastal SCBA as SCM, hence creating awareness in the EAC countries, cement manufacturing industries, and the possibility of using the coastal SCBA in manufacturing the pozzolana cement.

2 Materials and methods

2.1 Fine aggregates (FA) and coarse aggregates (CA)

The FA used was natural sand from River Kitui, Kenya. The sand belonged to the category of fine aggregate grading zone II as per IS 383–2016. The CA were crushed stones from Ndarugo Quarry, Kenya, with a maximum nominal size of 20 mm. The particle size distribution for FA and CA is well illustrated in Fig. 2. The sample collection areas are as indicated in the geographical map of Fig. 1. The physical properties of FA and CA, are shown in Table 1.

2.2 Particle size distribution curves for SCBA, CA, and FA

The particle size distribution of SCBA, CA, and FA varied with sieve sizes as shown in Fig. 2.

Figure 2a shows the particle size distribution of the SCBA, ranging from 75 to 425 µm, with D_{10}, D_{50}, and D_{90} of 102.27, 199.92, and 351.45 um respectively. Figure 2b shows the particle size distribution of CA ranging from <6.3 to 28 mm with D_{10}, D_{50}, and D_{90} of 10.59, 14.54, and 18.94 mm respectively. The particle size distribution of FA ranged from <0.15 to 14 mm with D_{10}, D_{50}, and D_{90} of 0.23, 1.20, and 18.94 mm respectively. The D_{10}, D_{50}, and D_{90} values indicated that SCBA, CA, and FA had a wide range of particles, which optimized the mix designs as was observed from the concrete strength realised. The strength was higher than the target strength.

2.3 Mixture water and Portland cement

Tap water was used in casting and curing. CEM I/42.5N cement was used.

2.4 Sugar cane bagasse ash (SCBA)

The SCBA was oven-dried for 24 h at 105 °C. Dry samples have better heat transfer characteristics than moist samples [32–34]. Hence pre-heating at this temperature ensured moisture removal. The dry SCBA was then loaded into the steel furnace tray and then calcined at 600 °C for 3 h in a muffle furnace in two stages. Initially, it was calcined for 1 h and then allowed to cool to room temperature. After cooling, the SCBA was uniformly mixed. The uniformly mixed SCBA was subsequently re-calcined at the same temperature for an additional 2 h. Once the second calcination process was complete, it was left to cool to room temperature. Thereafter, the cooled SCBA was sieved using 75 µm to get processed SCBA (SCBA-600). The 75 µm sieve used ensured that SCBA-600 had very fine grain sizes, as the finer the grains the better the materials' mechanical strength [35]. The images of raw and SCBA-600 are shown in Fig. 3 and the physical properties are shown in Table 1.

2.5 Mix design

IS 10262-2009 and IS 456 were adopted. The aggregates and binders' physical properties were as presented in Table 1. Standard strength concrete, M25, mild exposure, was designed. Table 2 indicates all the mix details.

The partial replacement levels of 0, 10, 20, and 30% were chosen based on the literature reviewed [1, 8, 15–18].

2.6 Mixing, vibrating, casting and curing (ASTM C-192)

Four batches of SCBA doses (0%, 10%, 20%, and 30%) were made. First, SCBA-600 was dry-mixed with PC for uniformity (the binder), the mixer was then lubricated with water to prevent absorption. CA and partial water were then added, and mixed for 6 min. FA, binder, and the remaining water then followed. The ingredients were mixed for 5 min, rested for 4 min, and mixed again for 4 min. The resulting concrete was transferred to a damp pan, remixed,

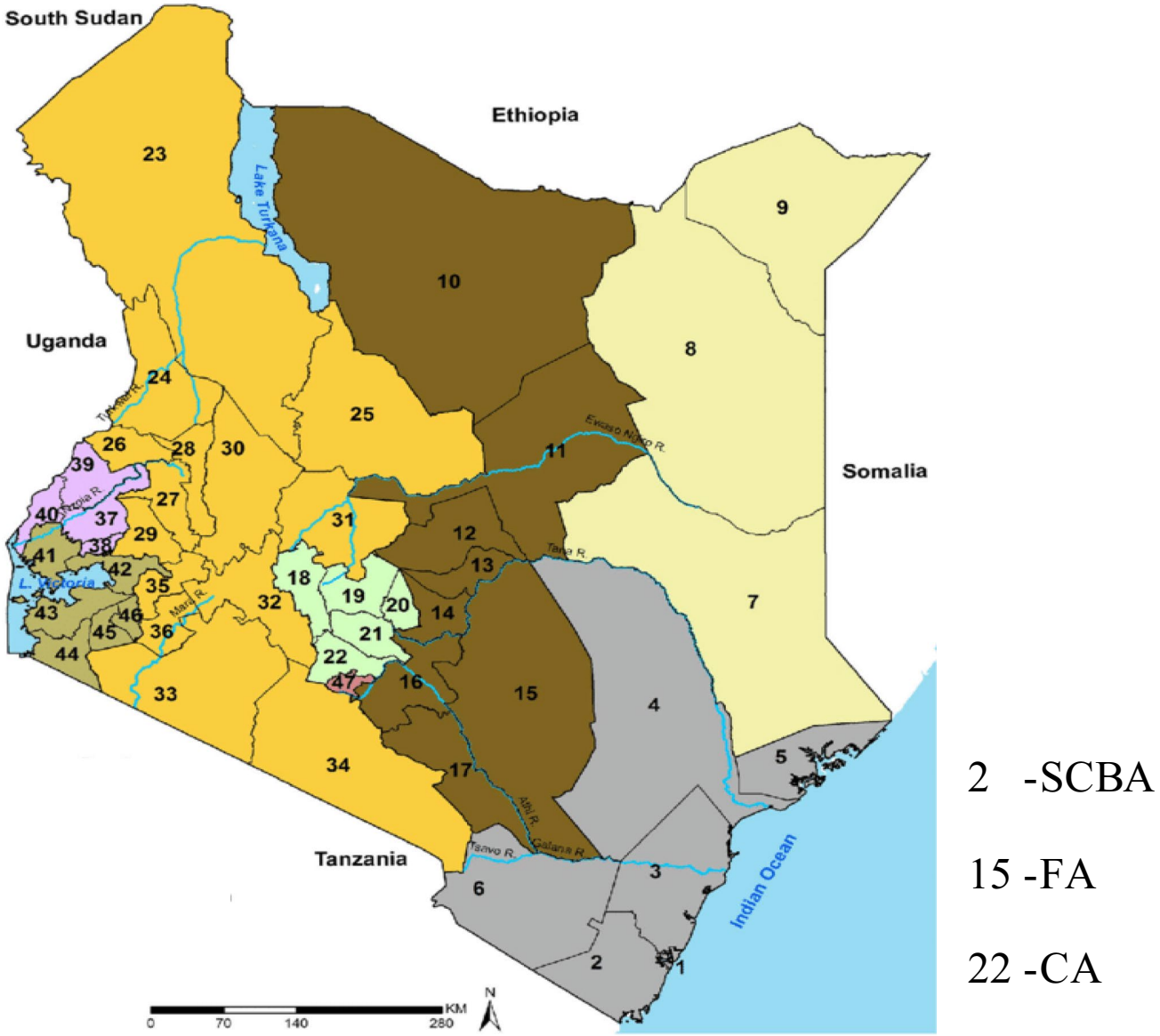

Fig. 1 Kenya geographical map indicating the sample areas for SCBA, FA, and CA

Table 1 Physical properties of FA, CA, raw SCBA, processed SCBA at 600 °C (SCBA-600), and CEM I/42.5N

Name	FA	CA	Raw-SCBA	SCBA-600	CEM I/42.5N	Standard
Colour and texture	Caramel	Grey and smooth	Black	Light off white	Grey	–
Shape	Rounded	Angular	Varied	Varied	Varied	–
Specific gravity	2.64	2.84	–	2.31	3.15	IS 2386-(1) & (3)
Max. nominal aggregate size	4.75 mm	20 mm	–	–	–	IS 383:2016
Water absorption	2.20	0.40	–	–	–	IS 2386-(3)
Moisture content	1.70	0.20	–	–	–	IS 2386-(3)
Fineness modulus	2.52	–	–	1.17		IS 2386-(1) and IS 383:2016

and placed into moulds (150 mm cubes and 500 × 100 × 100 mm prisms). This was followed by consolidation with a vibration table and smooth levelling. Moulds were demoulded after 24 h, and specimens were water-cured at room temperature and removed 1 day before testing.

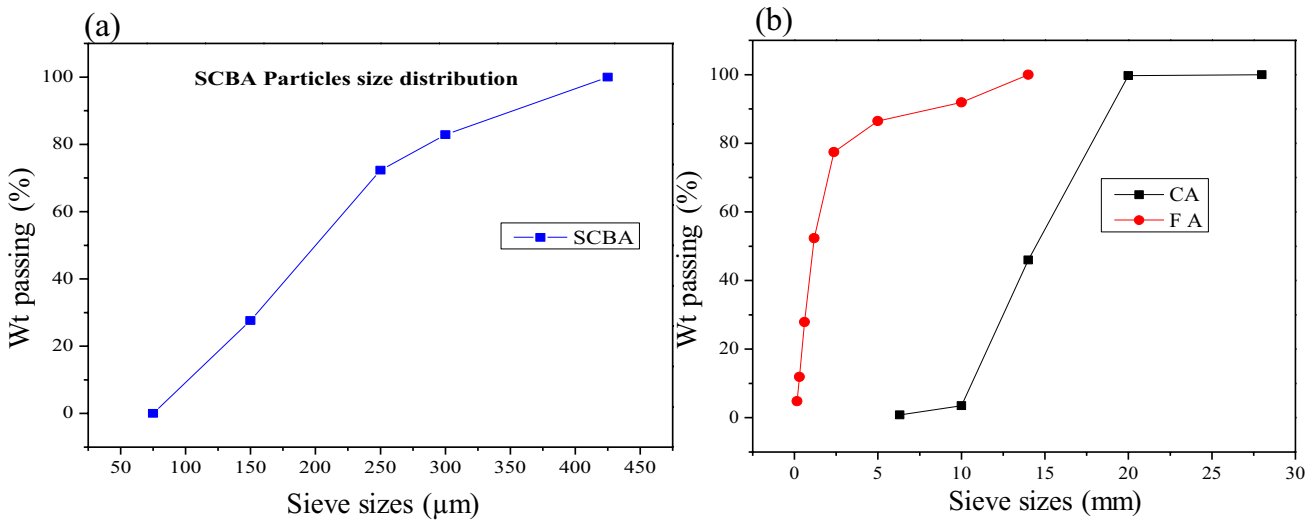

Fig. 2 The particle size distribution (PSD) curves for **a** SCBA and **b** CA and FA

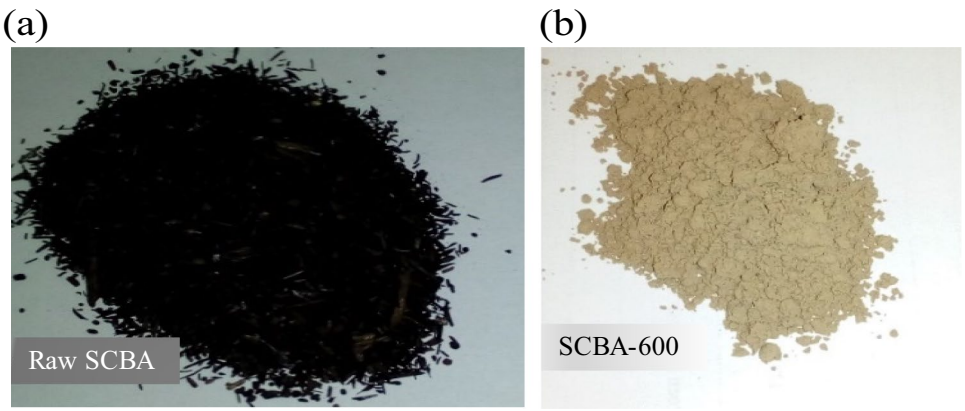

Fig. 3 The optical image of **a** raw SCBA and **b** SCBA-600

Table 2 Mix proportion with SCBA doses (kg/m^3)

Mix ID	% replacement	SCBA	Cement	Water	FA	CA	W/C
SCBA-0	0.0	0.00	372.00	186.00	698.23	1225.52	0.50
SCBA-10	10.0	37.20	334.80	186.00	694.21	1218.47	0.50
SCBA-20	20.0	74.40	297.60	186.00	690.20	1211.43	0.50
SCBA-30	30.0	111.6	260.40	186.00	686.19	1204.39	0.50

2.7 Compressive and flexural strength

Compressive and flexural strength tests were done after 28 days of curing. The compressive strength test was carried out as per ASTM C-39. The Controls Group Universal Tensile Machine (UTM) was used. The flexural strength test was carried out as per ASTM C78-00. The UTM model 50-C3012 of high stiffness flexural frame of 350 kN was used. These ASTM standards were preferred since these UTMs were calibrated against them.

2.8 Characterization methods

The microstructural properties were determined using X-ray diffraction (Shimadzu RD-7000 X-Ray Diffractometer, CuKα, λ = 1.5418 Å). The scan range was between 10° and 90° at a step size of 0.02° with a scanning speed of 2.00°/min. The surface morphology was determined using a scanning electron microscope (SEM) (Zeiss sigma series, sigma 300 VP). The elemental composition was determined using energy-dispersive X-ray spectroscopy (EDX). The chemical compounds were determined using an X-ray Fluorescence (XRF) Spectrometer (Shimadzu EDXRF 800HS).

3 Results and discussion

3.1 Portland cement phase identification-XRD analysis

The Portland cement received was compared against the International Crystal Structural Database (ICSD) standards as per Fig. 4. The major mineral phases realised with their respective phase angles and space groups are indicated in Table 3.

The major mineral phases identified as shown in Fig. 4 and Table 3 were alite, belite, celite, and millerites. These phases play a major role in concrete development. Alite phases have the highest composition followed by belite, celite, and lastly, millerite as indicated by the large number of their peak angles in Table 3. During hydration, alite rapidly and exothermically reacts with water to form calcium silicate hydrates (C-S-H) so does celite to form calcium aluminate hydrate (C-A-H) or ettringite. These contribute to early-stage concrete strength development [36]. Belite and millerite also react with water to form calcium silicate hydrate (C-S-H) and calcium ferrite hydrate (C-F-H), respectively. These former reactions are slow-paced and therefore contribute to the later stage of concrete strength development [37]. Moreover, as these reactions take place, there is also the production of calcium hydroxide (portlandite). Alite and belite produce more portlandite than celite and millerite due to their abundance in the cement sample. These cement hydration reactions are as in Eqs. 1–4 [37].

$$\underset{\text{(alite)}}{2(3CaO \cdot SiO_2)} + \underset{\text{(water)}}{6H_2O} \rightarrow \underset{\text{(C–S–H)}}{3CaO \cdot 2SiO_2 \cdot 3H_2O} + \underset{\text{(portlandite)}}{3Ca(OH)_2} \quad (1)$$

$$\underset{\text{(belite)}}{2(2CaO \cdot SiO_2)} + \underset{\text{(water)}}{4H_2O} \rightarrow \underset{\text{(C–S–H)}}{3CaO \cdot 2SiO_2 \cdot 3H_2O} + \underset{\text{(portlandite)}}{Ca(OH)_2} \quad (2)$$

$$\underset{\text{(celite)}}{3CaO \cdot Al_2O_3} + \underset{\text{(gypsum)}}{3CaSO_4} + \underset{\text{(water)}}{32H_2O} \rightarrow \underset{\text{(ettringite)}}{3Ca_6Al_2(SO_4)_3(OH)_{12} \cdot 26H_2O} \quad (3)$$

Ettringite further transforms to calcium monosulphoaluminate

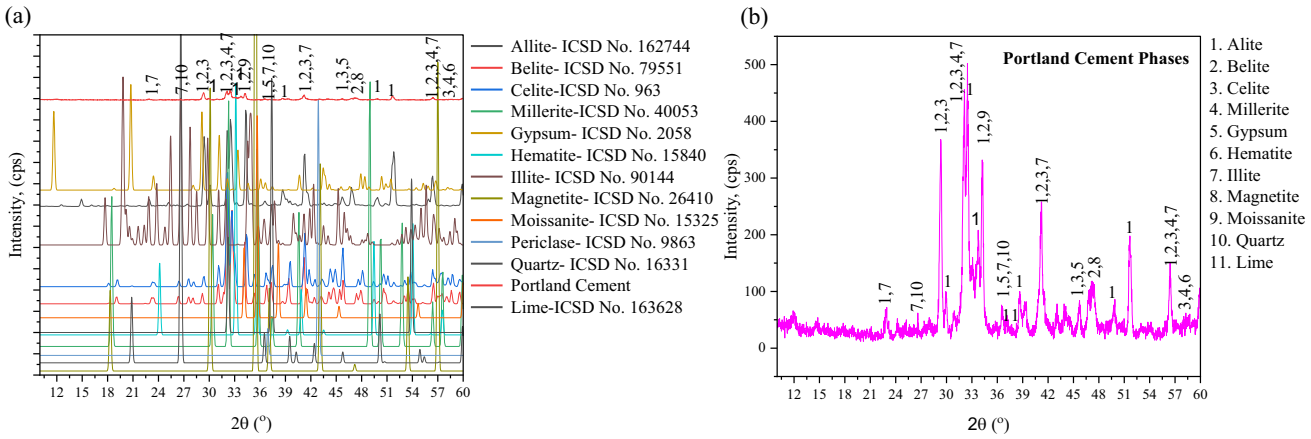

Fig. 4 **a** CEM I/42.5N XRD graph. **b** Enlarged CEM I/42.5N XRD graph

Table 3 CEM I/42.5N Portland cement mineral phases

Mineral phase	Space group	Cement chemist notation (CCN)	Chemical formula	Phase angle (2θ°)	
				Major	Minor
Alite	C1m1	C_3S	$3CaO{\cdot}SiO_2$	29.36, 32.08, 32.46, 34.22, 41.2, 51.66, 56.42	22.96, 29.94, 33.72, 36.54, 38.68, 45.64, 49.92
Belite	$P12_{1/n}1$	C_2S	$2CaO{\cdot}SiO_2$	29.36, 32.08, 34.22, 41.2, 56.42	47.22
Celite	Pa-3	C_3A	$3CaO{\cdot}Al_2O_3$	29.36, 32.08, 41.2, 56.42	45.64, 58.26
Millerite	Ibm2	C_4AF	$4CaO{\cdot}Al_2O_3{\cdot}Fe_2O_3$	32.08, 56.42	58.26
Gypsum	I 12/c1	–	Ca_2SO_4	–	36.54, 45.64
Hematite	R-3/cH	–	Fe_2O_3	–	58.26
Illite	C12/C1	–	$(K, H_3O)(Al, Mg, Fe)_2(Si, Al)_4O_{10}[(OH)_2{\cdot}(H_2O)]$	32.08, 41.2, 56.42	22.96, 26.64, 36.54
Magnetite	Fd3m	–	Fe_3O_4	–	47.22
Moissanite	R3mH	–	SiC	34.22	
Quartz	$P3_121$	–	SiO_2	–	26.64, 36.54
Lime	Fm-3m	–	CaO	36.6	–

The major diffraction peaks were observed at lower angles due to Bragg's law. The angle at which a peak occurs is related to the spacing between crystal lattice planes, and the intensity of the peak is related to the abundance and arrangement of atoms in those planes. Therefore the peaks identified indicate the abundance of these minerals in the sample

$$Ca_6Al_2(SO_4)_3(OH)_{12}\cdot 26H_2O + 2(3CaO\cdot Al_2O_3) + 4H_2O \rightarrow \underset{\text{(calcium monosulphoaluminate)}}{CaO\cdot Al_2O_3\cdot CaSO_4\cdot 12H_2O} \quad (4)$$

3.2 Raw-SCBA and SCBA-600 XRD analysis

For XRD analysis on SCBA, five major peaks were realized from the raw SCBA as shown in Fig. 5a. Additionally, upon calcination, ten major mineral phases of SCBA-600 were identified as shown in Fig. 5b; these mineral phases (for both raw and SCBA-600) realised with their respective phase angles and space groups are as indicated in Table 4.

From Fig. 5a, raw SCBA was calcined at 600 °C to activate its pozzolanic phases (silica, iron, and alumina), enhance its reactivity, remove any organic matter, and remove inert carbonaceous materials which do not contribute to pozzolanic reactions [1, 5]. The raw-SCBA was identified to have five major phases, cristobalite, hematite, illite, mullite, and quartz as shown in Fig. 5a and Table 4. On calcination, five additional mineral phases were identified; kaolinite, magnetite, moissanite, periclase, and metakaolinite as indicated in Fig. 5b and Table 4. The kaolinite changed to metakaolinite (a highly reactive pozzolana material) at this temperature [24, 38]. Hence having its phases in the SCBA-600 greatly improves its cementitious properties. The presence of silica in the mineral phase of cristobalite and quartz, iron oxide in the mineral phase of hematite and magnetite, and aluminium oxide in the mineral phases of mullite, illite, kaolinite and metakaolinite indicates that SCBA has pozzolanic properties since silica, alumina and iron are the major pozzolanic elements [39].

These findings were similar to reports of Abdalla et al. [1], and Kannur and Bore [39], who observed, quartz, cristobalite and hematite after calcination of raw SCBA. The crystallinity of the SCBA-600 is seen in its sharp peaks compared to raw SCBA in Fig. 5a and b. Silicates, alumina and iron are the active phases of pozzolans as presented in Table 4 [19]. These are the phases which react with portlandite from the cement hydration reactions in Eqs. 1–4, enhancing concrete strength development, durability and porosity reduction [36]. The high reactivity SCBA calcined at 600 °C enhances the density and bond strength of the cement matrix by acting as a micro-filler and producing additional ettringites, C-S-H, and C-A-H gels [15, 40]. Additionally, reduced carbon content due to calcination improves the compatibility of SCBA with other cement components [20, 21, 27].

3.3 Surface morphology and elemental composition analysis of PC

SEM image in Fig. 6a indicates the PC particle shapes are rectangular, spherical and irregular for 1, 2 and 3 particles respectively. Particle sizes also vary, 60, 45 and 15 µm, for 4, 5 and 6 particles respectively. There is non-uniformity in

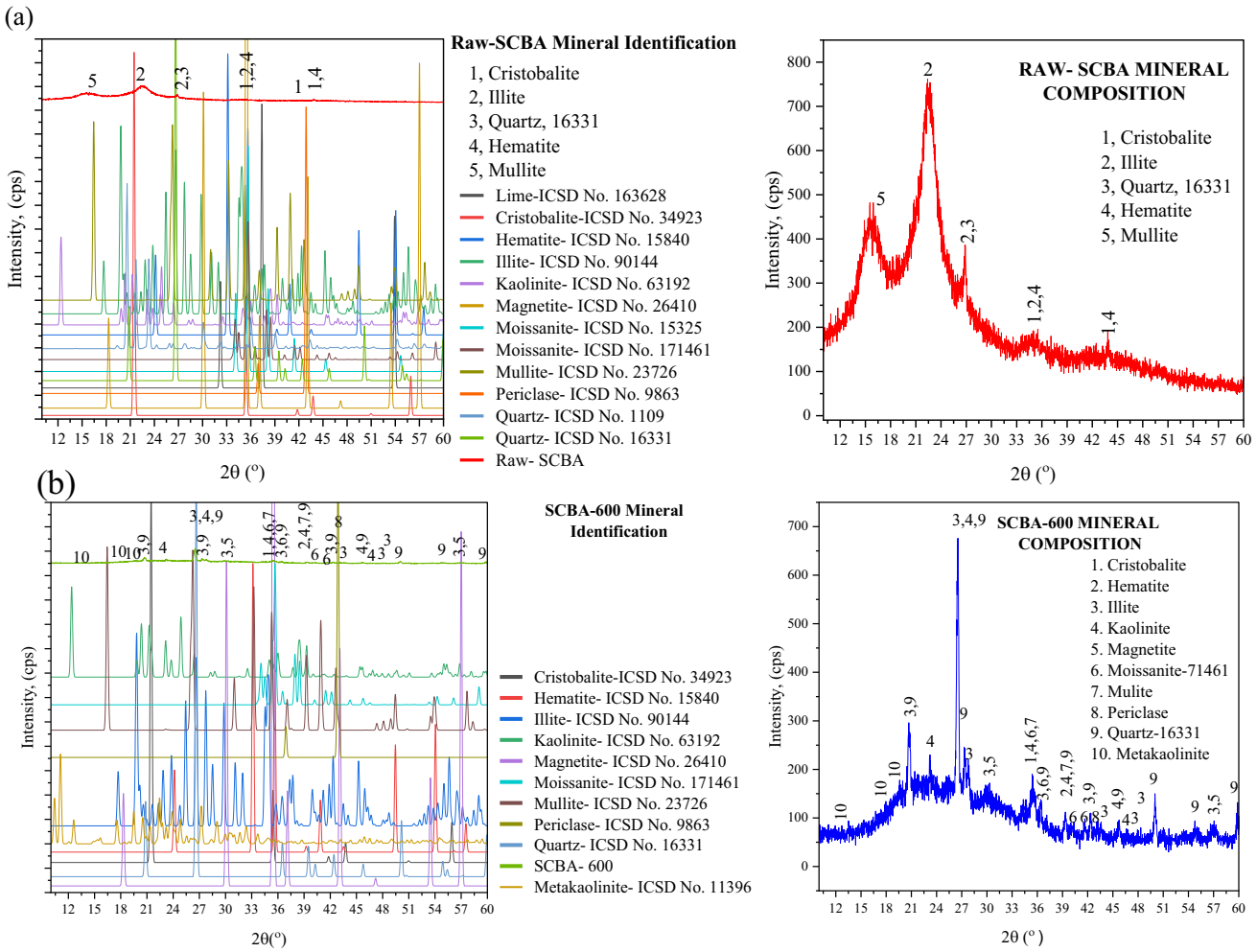

Fig. 5 Raw SCBA and SCBA-600 XRD graph. **a** XRD of Raw SCBA and **b** XRD of SCBA-600

Table 4 The raw SCBA and SCBA-600 mineral composition at different peak angles

Mineral phase	Space group	Chemical formula	Peaks angle (2θ°)	
			Raw SCBA	SCBA-600
Cristobalite	Fd3-mz	SiO_2	35.52, 43.84	35.38, 43.62
Hematite	R-3/cH	Fe_2O_3	35.52, 43.84	39.34, 43.62
Illite	C12/C1	$(KH_3O)(Al, Mg, Fe)_2(SiAl)_4O_{10}[(OH)_2(H_2O)]$	22.38, 26.84, 35.32	20.72, 26.54, 27.72, 30.14, 36.44, 42.26, 43.62, 48.08, 48.38, 57.1
Quartz 16331	$P3_121$	SiO_2	26.84	20.72, 26.54, 27.22, 36.44, 39.34, 40.14, 42.26 45.76, 50.02, 54.76, 59.92
Mullite	Pbam	$3Al_2O_3{\cdot}2SiO_2$	16.38	35.38, 39.34, 48.08, 42.62
Magnetite	Fd3m	Fe_3O_4	–	30.14, 43.24, 57.1
Moissanite, 71461	R3mH	SiC	–	35.38, 36.44, 40.14, 41.58
Periclase	Fm-3m	MgO	–	42.62
Kaolinite	C1	$Al_2Si_2O_5(OH)_4$	–	23.24, 26.54, 35.38, 39.34, 45.76, 46.82
Metakaolinite	P-1	$Al_2O_3{\cdot}2SiO_2$	–	12.66, 17.52, 19.44

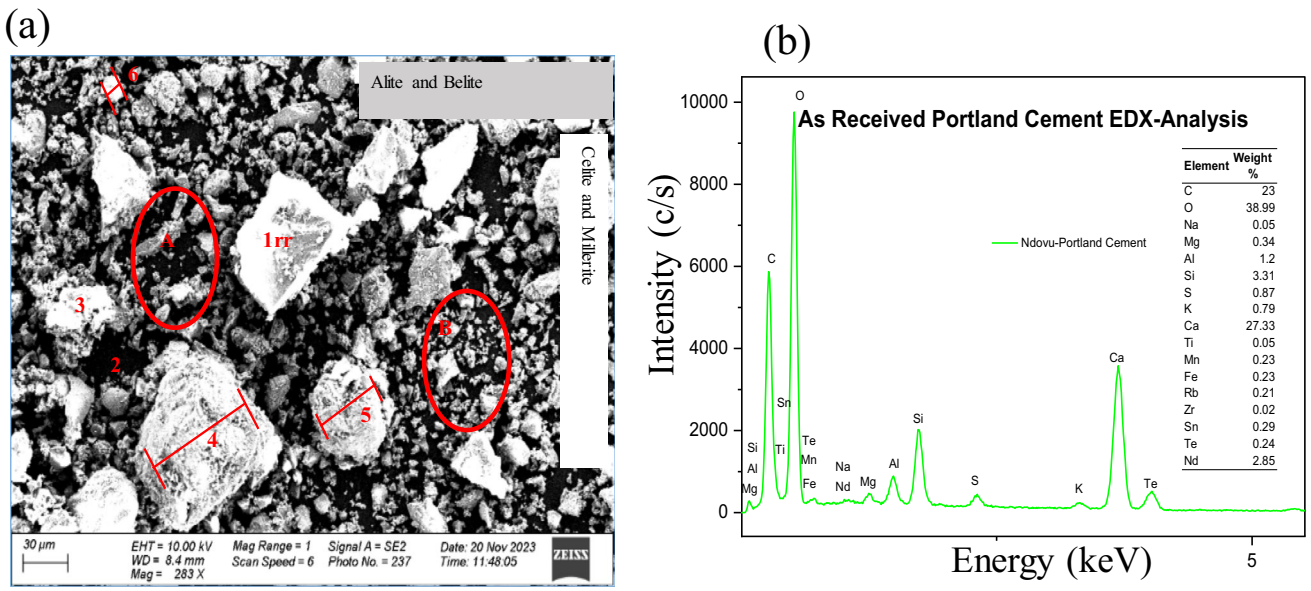

Fig. 6 **a** SEM image for PC. **b** EDX graph for PC

distribution density, sparsely in A and densely in B, hence unequal inter-particle distance. More so most of the particles have rough surface texture associated with voids and pores for particles 4 and 5. These rough particle surfaces can lead to good interlocking on materials mixing hence increasing the material binding property [16, 36]. Lastly, there is variation in particle brightness, alite and belite are mostly dull, and celite and millerite are bright. This is in agreement with previous reports of Stutzman and Leigh [41], and Paya et al. [42] while working on phase analysis of different compounds.

EDX is an analytical method, that is used to determine elemental composition and operates on the concept that, each voltage pulse directly relates to the energy of the incoming X-ray photon [5]. The major PC elemental concentrations are shown in Fig. 6 with major elements of O, Ca, C, Si, Nd, and Al and minor elements of S, K, Mg, Sn, Te, Mn, Fe, Rb, Ti, Na, and Zr. The percentage of elemental composition is shown in the inset of Fig. 6b.

3.4 Surface morphology and elemental composition of SCBA

Figure 7a shows the surface morphology of raw SCBA. The images reveal the fibrous (particle B) and prismatic (particle D) nature of the particles with size distributions ranging between 200 and 2000 µm as indicated by particles A and B respectively, this similar observation was also opined by Bheel et al. [43]. The fibrous and prismatic nature shows that they are carbonaceous and siliceous respectively [44]. The particles' surface textures are rough (particle E) since they have the appearance of pores/voids. There is also variation in brightness, indicating a difference in particle composition, the dull areas contain the mineral phases of quartz, mullite, illite, and cristobalite while the bright areas contain hematite. SCBA-600 showed particle shapes to be spherically elongated irregular and fibrous as indicated in Fig. 7c. A similar observation was also made by Abdala et al. [5] so is Kannur and Chore [39]. Particle sizes varied between 15 (C) and 60 µm (D) as was also reported in [1]. The particles' surface texture was generally rough, for particles A and F (Fig. 7c). Some particles were bright (particle F) and others were dull (particle D), due to the variation in the mineral composition. The bight particles are, hematite, magnetite, and periclase since their elements have relatively high atomic numbers compared to the dull particles; kaolinite, illite, mullite, quartz and moissanite [45].

The elemental analysis of raw SCBA is shown in Fig. 7b. The major elements were C and O and the minor elements were; Na, Mg, Al, Si, S, K, Ti, Mn, Fe, Rb, Zr, Sn, Te and Nd. As shown in Fig. 7d, the major elements present in the SCBA-600 were O, C, Si, Al, Ca, Fe and Nd. The minor elements were Na, Mg, S, Ti, Mn, Rb, Zr, Sn and Te. The percentage elemental composition is shown in the inset of Fig. 7b and d. From the major elements identified, raw SCBA had no pozzolanic elements, Si, Al and Fe. However, on calcination to SCBA-600, these pozzolanic elements were identified in large quantities. This is a clear indication that using raw SCBA in concrete production may lead to substandard concrete, inadequate strength and compromised durability.

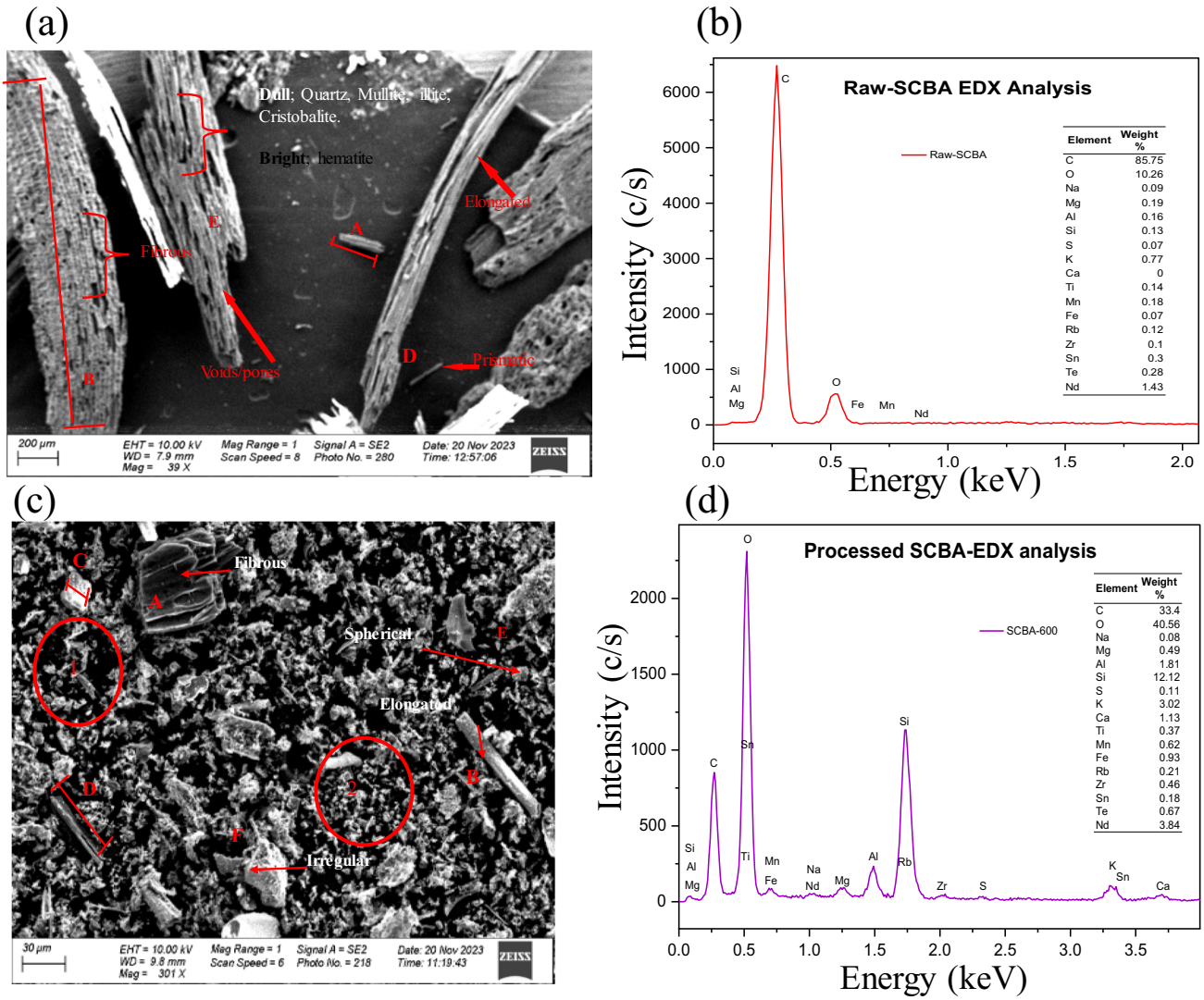

Fig. 7 **a** SEM image for raw SCBA, **b** EDX graph for raw SCBA. **c** SEM image for SCBA-600, **d** EDX graph for SCBA-600

3.5 Surface morphology and elemental composition of hydrated concrete showing optimum results (concrete made from the mix of SCBA-20)

Figure 8 shows the optical image of the produced SCBA concrete. The concrete surfaces were smooth on physical touch. This is mainly due to the fine particle size of the SCBA as shown from the particle size distribution curve in Fig. 2 and the finesse modulus of 1.17 in Table 1.

Figure 9 shows the surface morphology and elemental composition of hydrated concrete under SEM. The concrete surface texture appears rough due to aggregate distribution. There is variation in brightness. The area labelled A appears darker compared to area B, due to mineral compounds ettringite and portlandite respectively. This is because elements making portladite have less atomic number leading to weaker electron scattering compared to ettringite [45]. The elemental composition of hydrated powdered SCBA-20 concrete mix has major elements of O, C, Ca, Si, Al, Na and Nd. The minor elements were, K, Te, Rb, Fe, S, Sn, Mg, Mn, Ti, and Zr. Their percentage distribution is shown in the inset of Fig. 9b.

Fig. 8 Optical images for the produced SCBA concrete blocks

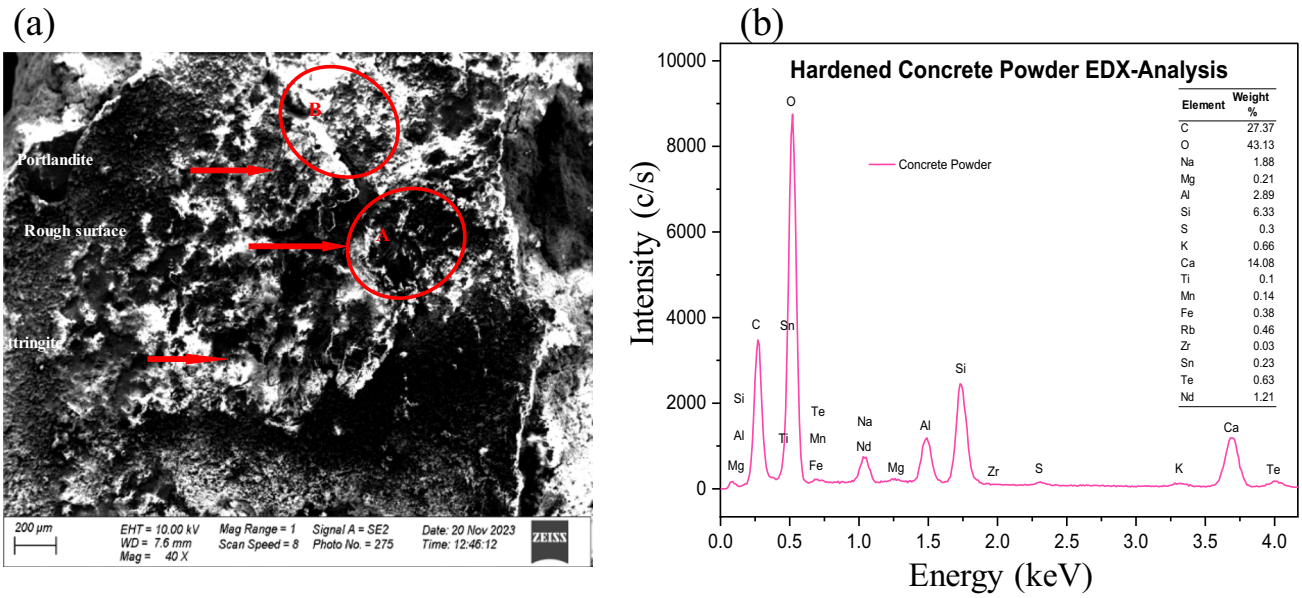

Fig. 9 **a** SEM image for SCBA concrete and hydration products, **b** EDX graph for SCBA concrete

3.6 XRF analysis

To quantify the chemical compounds, the XRF technique was used. The major PC chemical oxides observed were; CaO, SiO_2, Al_2O_3 and Fe_2O_3. The minor oxides were; K_2O, MnO, TiO_2, SO_3, ZrO_2, SrO, RbO_2 and NbO. The major SCBA-600 oxides were; SiO_2, K_2O, Fe_2O_3, Al_2O_3, CaO, P_2O_5 and MnO. The minor oxides were; TiO, SO_3, ZrO_2, ZnO, SrO, NiO, RbO_2, CuO, and NbO. The percentage distribution of all the major and minor compounds is summarized in Table 5.

These results are in agreement with EDX and XRD analysis showing silica, alumina and iron as the major composites of SCBA-600. These elements form the reactive phases of SCBA-600 which take part in hydration reactions during concrete manufacturing. They eliminate portlandite in the concrete matrix to enhance concrete strength and reduce water penetrability [5, 8, 15]. The total summation wt% of SiO_2, Al_2O_3, and Fe_2O_3 compound is 70.6%. Hence SCBA-600 is class N or F pozzolan as per ASTM C618-12a since the summation of its SiO_2, Al_2O_3, and Fe_2O_3 is above 70%, the maximum sulphur trioxide is less than 3% and its LOI is less than 10% as per ASTM C 618 [46].

Table 5 Portland cement and SCBA-600 chemical oxides

Chemical composition	CEM I/42.5N	SCBA-600
	Concentration wt% m/m	
Silicon dioxide, SiO_2	17.068	44.331
Aluminium oxide, Al_2O_3	3.695	12.819
Iron oxide, Fe_2O_3	3.095	13.450
Potassium oxide, K_2O	0.371	21.623
Calcium oxide, CaO	71.592	3.271
Manganese oxide, Mn	0.054	1.072
Titanium oxide, Ti_2O	0.225	0.833
Sulphur trioxide, SO_3	2.644	0.124
Zirconium dioxide, ZrO_2	0.033	0.104
Strontium oxide, SrO	0.115	0.035
Rubidium oxide, RbO_2	0.003	0.020
Niobium oxide, NbO	0.005	0.012
Phosphorous pentoxide, P_2O_5	–	2.225
Zinc oxide, ZnO	–	0.042
Nickel oxide, NiO	–	0.020
Copper oxide, CuO	–	0.018

Loss on ignition (LOI) for SCBA-600 was found to be 4.80%

3.7 Pozzolanicity activity

Pozzolanicity is the ability of certain materials to react chemically with portlandite from cement hydration, in the presence of water to form compounds with cement properties which contribute to concrete strength and durability [14, 47].

There is a constant reduction in SAI elements in the hydrated concrete when compared to the summation of the SAI elements of SCBA-600 and Portland cement as illustrated in Table 6. The reduction is due to, dilution effects, when the binder was mixed with aggregates and water, the overall concentration of SAI in the resulting concrete mixture decreased [16, 17, 48]. Moreover, chemical reactions of these elements leading to the formation of new compounds of C-S-H, C-A-H, and ettringite also elevated their depletion [1, 37]. The reduced SAI elements to 6.33, 2.89, and 0.38% are a clear indication of pozzolanic reactions for SCBA-600 leading to the formation of these compounds which enhance concrete strength, reduce porosity and reduce water absorption [27].

3.7.1 Pozzolanic activity index (PAI)

A PAI of 75% or higher (per ASTM C 618) indicates the material has adequate pozzolanic activity to be considered a viable supplementary cementitious material [48]. The PAI of SCBA-600 concrete was calculated as follows;

$$\mathrm{PAI} = (\mathrm{A}/\mathrm{B}) \times 100\%.$$

$$(39.75/36.25) \times 100\% = 109.66\%$$

Table 6 Comparison of silicon, aluminium and iron (SAI) elements of hydrated concrete and raw concrete materials

EDX SAI elemental analysis (wt%)			
	Silicon	Aluminium	Iron
CEM I/42.5N + SCBA-600	15.43	3.01	1.16
Hydrated Concrete made from the mix of SCBA-20	6.33	2.89	0.38

These SAI percentages are derived from the EDX analysis from Figs. 6b, 7d and 9b

A is the average compressive strength of SCBA-600 concrete while B is the average compressive strength of SCBA-0 (control mix). SCBA-600 concrete has a PAI of 109.66%. This is greater than 75% hence SCBA-600 is a viable SCM.

3.7.2 Pozzolanic reactions

During SCBA concrete production, portlandite produced during cement phases hydration reacts with silica and alumina in the SCBA-600 to give, calcium aluminium hydrate (C-A-H), calcium silicate hydrate (C-S-H), and calcium aluminium silicon hydrate (C-A-S-H), as shown in Eqs. 5 and 6 [1]. These reactions lead to improved paste and aggregate interlocking [49]. Hence, the proliferation of fewer pores in the concrete matrix leads to good mechanical properties [31].

$$Al_2O_3 + Ca(OH)_2 + H_2O = C{-}A{-}H \tag{5}$$

$$SiO_2 + Ca(OH)_2 + H_2O = C{-}S{-}H \tag{6}$$

$$SiO_2 + H_2O + Ca(OH)_2 + Al_2O_3 = C{-}A{-}S{-}H \tag{7}$$

3.8 Mechanical concrete properties

Concrete mechanical properties were investigated after 28 days of casting and curing since most concrete mixes had reached a significant portion of their ultimate strength [40]. Testing at 28 days gives a good indication of strength potential and suitability for the intended use. The results are shown, in Fig. 10a and b. The best mechanical properties were that of the SCBA-20 mix design. The analysis of compressive and flexural strength after 28 days of concrete curing is summarised in Table 7. From the four mixes designed, SCBA-0, SCBA-10, SCBA-20 and SCBA-30, forty samples were prepared (cubes of 150 mm for compressive strength test, twenty in number and the prism of $100 \times 100 \times 500$ mm for flexural strength test, twenty in number). The slump values for SCBA-0, SCBA-10, SCBA-20 and SCBA-30 mixes were 106, 87, 98, and 76 mm respectively.

3.8.1 Compressive strength

Table 7 and Fig. 10a, indicate greater variations of the compressive strength from the control mix (SCBA-0). The mix of SCBA-10 has a strength variation of 6.34% lower than the control mix as shown in Fig. 10a and Table 7. This is attributed

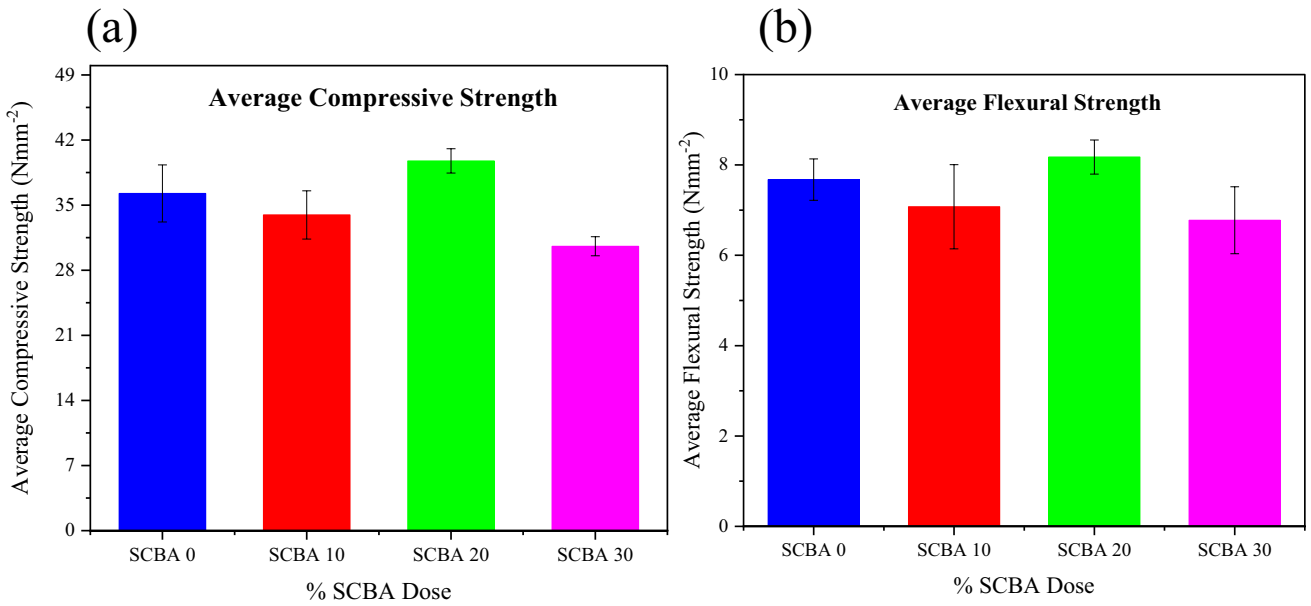

Fig. 10 **a** Average compressive and **b** average flexural strength at 28 days of concrete curing

Table 7 Compressive and flexural strength after 28 days of concrete curing

Mix	Replacement level (%)	Compressive strength (N mm^{-2})	Strength variation from control mix (N mm^{-2})		Flexural strength (N mm^{-2})	Strength variation from control mix (%)		Remarks
			Compressive	Flexural		Compressive	Flexural	
SCBA-0	0	36.25	0.00	0.00	7.68	0.00	0.00	Constant
SCBA-10	10	33.95	−2.30	−0.6	7.08	−6.34	−7.81	Lower
SCBA-20	20	39.75	3.50	0.5	8.18	9.65	6.51	Higher
SCBA-30	30	30.57	−5.68	−0.9	6.78	−15.66	−11.72	Lowest

(−) indicates strength lower than the control mix. (+) indicates strength higher than the control mix. Examining closely the relationship between the flexural strength (f_r) and the compressive strength (f_c), a relationship similar to $f_r = 0.20f_c$ is realised [50]. This is attributed to high-quality aggregates and binder material (SCBA-600 and CEM1/4.2) used in the mix design, so is good curing conditions

to weaker adhesive bonds introduced by excess portlandite (calcium hydroxide) [8]. Portlandite is relatively weak and contributes little to the strength of concrete therefore, its presence in the concrete matrix reduces the concrete strength, concurring with the current observation reported in Kannur and Chore [8]. Most of the SCBA introduced into the mix at a dosage of 10% had all been depleted during the pozzolanic reactions as indicated in Eqs. 5–7. Some excess portlandite formed a film around slower-reacting cement phases (belite and celite) stopping further formations of C-S-H and C-A-H gels which enhances the concrete strength leading to a comparable weak concrete [14, 30] The mix of SCBA-20 had a strength variation of 9.65% higher than the control mix. This mix depicted the optimum strength. This is attributed to the optimum amount of SCBA present in the binder matrix to react with most of the portlandite formed, as established earlier, SCBA has reactive pozzolanic phases of alumina and silica [17, 30, 31]. These phases reacted with most of the portlandite formed during the initial hydration reactions involving the cement phases of alite and celite at early age concrete strength development [36] and all the portlandite produced at late stage strength development from the slow-paced cement phases of belite and millerite [36, 37]. This action led to the optimum formation of C-S-H, C-A-H, and C-A-S-H gels as per Eqs. 5–7, which enhanced the concrete strength by increasing concrete matrix densification [36, 47]. Finally, the mix of SCBA-30 with a strength variation of 15.66% lower than the control mix, had the least strength. This is attributed to the excess SCBA in the mix leading to the dilution of the cement in the mix. Due to the inert nature of the SCBA [14], the excess could not take part in any further reaction and hence acted as inert fillers within the concrete matrix. This led to poor interfacial bonding between SCBA-600 particles, and cement matrix aggregates leading to weaker bonds [51].

3.8.2 Flexural strength

Table 7 and Fig. 10b indicate the results of the flexural strength showing three distinct variations from the control mix. The variation of the flexural strength among the four mixes can be attributed to the bonding in the Interfacial Transition Zone (ITZ) of the concrete matrix [14]. The ITZ often has a higher concentration of voids, micro-cracks, and weaker bonds compared to the bulk cement paste. Hence it's a zone of reduced strength, making it a potential weak link in the concrete matrix [49]. Moreover, if the ITZ is poorly formed or weakened due to inadequate bonding between the cement pastes and aggregate, it may contribute to reduced flexural strength [36, 51]. This inadequate bonding is realised when there is comparably more portlandite in the concrete matrix [14]. On the other hand, a well-bonded and strong ITZ can enhance the overall performance of the concrete in flexural loading. The pozzolanic reactions (silica, alumina and iron present in the SCBA-600 reacting with the portlandite) may lead to the refinement of the microstructure [22, 48]. This happens by reducing the size of the pores and enhancing the density of the ITZ, increasing the concrete adhesion [8]. This refinement results in a denser and less porous ITZ, hence improving the bond strength between aggregates and cement paste [49]. When the SCBA was mixed with cement paste, upon pozzolanic reactions, C-A-H, C-S-H, and C-A-S-H gels were formed, as indicated in Eqs. 5–7. These gels formed influenced the ITZ as filler effects at a nano/micro-level, reducing the thickness of the ITZ by filling in the pores and micro-cracks which might have developed during the rapid pozzolanic reaction processes. The filling enhances the regional microstructures within these ITZs [14, 51]. Hence influencing the concrete flexural strength.

In the mix of SCBA-10 where the variation of strength was 7.81% lower than the control mix, there was less SCBA-600 present in the mix to enhance the production of enough C-S-H and C-A-H (ettringite) gels which would enhance the interfacial transition zone (ITZ) by filling in pores and micro cracks to optimize the flexural strength. SCBA-20 mix

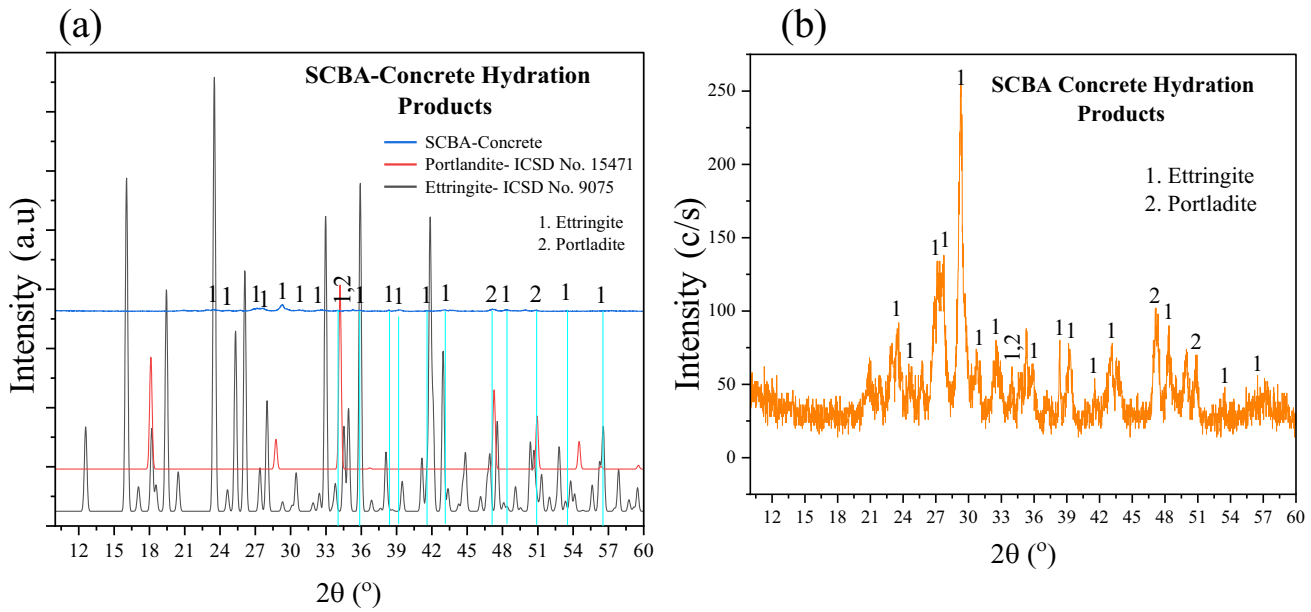

Fig. 11 **a** Powdered SCBA-600 concrete phase's identification using ICSD standards, **b** identified crystallization phases of powdered SCBA-600 concrete

Table 8 Powdered SCBA-600 concrete hydration products at different peak angles

Mineral phase	Space group	Chemical formula	Peaks angle (2θ°)
Ettringite	P63	$Ca_6Al_2(SO_4)3(OH)_{12}{\cdot}26H_2O$	23.6, 24.74, 27.12, 27.74, 29.26, 30.7, 32.52, 33.98, 35.82, 38.36, 39.16, 41.56, 43.16, 48.36, 53.48, 56.48
Portlandite	P3-m1	$Ca(OH)_2$	33.98, 47.12, 50.92

achieved optimum flexural strength, 6.51% above the control mix. This was due to having enough quantity of the SCBA-600, which enhanced the optimum production of the C-S-H gel and ettringite. The C-S-H gel fills in voids, reduces porosity, and increases the strength of the ITZ, making the overall concrete stronger and more durable. These filled the voids and micro-cracks substituting weaker portlandite layers leading to stronger ITZ bonds between the cement paste and the aggregates. The SCBA-30 mix had the least strength, 11.72% lower than the control mix. This is due to, increased porosity, reduced ITZ bonds, and incomplete pozzolanic reactions due to an over-supply of the inert SCBA-600 in the concrete matrix [8, 14].

3.9 SCBA-600 concrete hydration products

After carrying out the concrete mix design with SCBA-600 at 0, 10, 20, and 30% dosages and testing for compressive and flexural strength, concrete mix with a 20% dose of SCBA-600 achieved the highest strength, with a compressive strength that is 3.5 N/mm^2 higher and a flexural strength that is 0.5 N/mm^2 higher than those of the control mix. The absolute control mix values were at 36.25 and 7.68 N/mm^2 for compressive and flexural strength respectively as indicated in Fig. 10 and Table 7. This mix became of interest to this study and was subjected to X-ray diffraction analysis for the hydration products. Figure 11 shows these hydration products' identification using ICSD standards graphs. The products identified were calcium aluminate hydrate (ettringite) and portlandite, with ettringite in large quantities in relation to portlandite as shown in Fig. 11b. These products showed different peak angles and space groups as summarized in Table 8 and played a critical role in the concrete strength development for this mix. This mix had the highest strength since it had a lot of ettringite, which enhanced the strength at late age development [14], and less adhesive portlandite which increases porosity within the concrete matrix [8].

4 Conclusion

In this contribution, we have demonstrated that SCBA available along the Kenya coast can positively influence the mechanical properties of the hardened concrete. In particular;

1. Calcining SCBA above 600 °C, improves its pozzolanic properties as shown by the pozzolanic activity index of 109.66%. This was done by; reducing non-reactive carbon sites and removal of impurities as indicated by the loss on ignition of 4.80%, increasing the reactive silica, alumina, and iron content to 44.331, 12.819, and 13.450%, reducing particle size, and increasing surface area as indicated by the fineness modulus of 1.17.
2. Kenya coastal SCBA is classified as class N or F pozzolan (since the summation of its silica, alumina and iron components is above 70%, the maximum percentage of sulphur trioxide is less than 3% and its LOI is less than 10% as per ASTM C 618). This implies that this SCBA-600 can be used in applications requiring rapid strength gain and resistance to aggressive chemicals. The pozzolanic activity index of 109.66% also affirms that SCBA-600 is a viable SCM since 109.66% > 75% stated in the ASTM C-618.
3. Most literature reviewed had optimised concrete strength at 10% cement replacement. In this study, the concrete had optimised strength greater than the design target strength at 20% cement replacement. This may be attributed to the good quality of the SCBA-600 and the ideal environment upon which the mix design was carried out. This is indicative that Kenya coastal SCBA has great potential for cement replacement and hence a great solution to carbon mitigation.

5 Recommendations

A further study on the following areas is recommended for a full understanding of the Kenya coastal SCBA for Portland pozzolana cement (PPC) production.

1. The influence of SCBA on concrete penetrability, in terms of gas permeability, and chloride ion penetration, its effects on carbonation and carbonation prediction model.
2. Study on the sustainability and environmental effects of the Kenya coast SCBA, in terms of actual CO_2 produced during its preparation hence its economic viability (life cycle analysis).

This research focussed on characterising the Kenya coastal sugarcane bagasse ash, improving it by controlled calcination, and using it to design a standard-strength concrete. This SCBA-manufactured concrete showed excellent strength development. Therefore, the adoption of this study by cement industry policymakers will lead to the value addition of the SCBA waste by; reducing SCBA waste disposal in landfills thereby creating a circular economy, and reducing carbon emissions associated with the PC production chain by partially replacing PC with this SCBA up to 20%. Simultaneously this will increase resource productivity and longevity. In line with this, the achievement of sustainable development goals (SDGs) 11 (sustainable cities and communities) and 13 (climate action) is attainable.

Acknowledgements The authors acknowledge the support of the East Africa Community Scholarship, sponsored by KFW Germany and administered through the Inter-University Council of East Africa (IUCEA). We further acknowledge Kyambogo University Competitive research grants for support.

Author contributions E.P. Mukhokosi: Conceptualisation, Supervision, Investigation, Writing—review & editing. E.N.: Conceptualisation, Investigation, Formal analysis, Writing—original draft. S.O.: Supervision, Writing—review & editing.

Data availability The datasets generated during and/or analysed during the current study are available from the corresponding author on reasonable request.

Declarations

Ethics approval There is no known ethical concern regarding this study.

Competing interests The authors declare no competing interests.

References

1. Abdalla TA, Koteng DO, Shitote SM, Matallah M. Mechanical properties of eco-friendly concrete made with sugarcane bagasse ash. Civ Eng J. 2022;8:1227–39. https://doi.org/10.28991/CEJ-2022-08-06-010.
2. Mehta PK. Reducing the environmental impact of concrete. Concr Int. 2001;23:61–6.
3. Eid MS, Saleh HM. Characterizations of cement and modern sustainable concrete incorporating different waste additives. London: Intechopen; 2021. p. 1–15.
4. Kumari A, Sheo K. Experimental study on partial replacement of cement by sugarcane bagasse ash (SCBA). Int J Innov Res Sci Eng Technol. 2015;4:5161–9. https://doi.org/10.15680/IJIRSET.2015.0407017.
5. Abdalla TA, Koteng DO, Shitote SM, Matallah M. Mechanical and durability properties of concrete incorporating silica fume and a high volume of sugarcane bagasse ash. Results Eng. 2022;16: 100666. https://doi.org/10.1016/j.rineng.2022.100666.
6. Farfan J, Fasihi M, Breyer C. Trends in the global cement industry and opportunities for long-term sustainable CCU potential for Power-to-X. J Clean Prod. 2019;217:821–35. https://doi.org/10.1016/j.jclepro.2019.01.226.
7. Andrew RM. Global CO_2 emissions from cement production, 1928–2017. 1 Introduction to previous estimates of global cement emissions. Earth Syst Sci Data. 2021;10:1–20.
8. Kannur B, Chore HS. Strength and durability study of low-fines self-consolidating concrete as a pavement material using fly ash and bagasse ash. Eur J Environ Civ Eng. 2023;27:3507–24. https://doi.org/10.1080/19648189.2022.2140207.
9. Li J, Li S, Peng L, Chen B. A new method to rapidly evaluate the activity of volcanic ash materials. Cem Concr Compos. 2023;135: 104833. https://doi.org/10.1016/j.cemconcomp.2022.104833.
10. Rahman SA, Dodd A, Khair S, Shaikh FUA, Sarker PK, Hosan A. Assessment of lithium slag as a supplementary cementitious material: pozzolanic activity and microstructure development. Cem Concr Compos. 2023;143: 105262. https://doi.org/10.1016/j.cemconcomp.2023.105262.
11. Rudić O, Ukrainczyk N, Krüger M, Tritthart J, Juhart J. Efficiency of limestone in clinker-reduced binders: consideration of water-binder ratio, capillary porosity and compressive strength. Constr Build Mater. 2023;386: 131594. https://doi.org/10.1016/j.conbuildmat.2023.131594.
12. Ascensão G, Farinini E, Ferreira VM, Leardi R. Development of eco-efficient limestone calcined clay cement (LC3) mortars by a multi-step experimental design. Chemom Intell Lab Syst. 2024;253: 105195. https://doi.org/10.1016/j.chemolab.2024.105195.
13. Iqbal MA, Sahar UU, Bahrami A, Yaseen N. Development of sugarcane bagasse ash blended cementitious composites reinforced with carbon nanotubes and polypropylene fibers. J Compos Sci. 2024;8:94. https://doi.org/10.3390/jcs8030094.
14. Bersisa A, Zekaria A. Assessment of the mechanical properties of bagasse ash concrete. Eng Sci. 2021;6:39. https://doi.org/10.11648/j.es.20210603.12.
15. Girma M, Asteray B. Fresh, mechanical, and microstructural properties investigation on the combined effect of biomedical waste incinerator ash and bagasse ash for high-strength concrete. Adv Mater Sci Eng. 2022;2022:5685372. https://doi.org/10.1155/2022/5685372.
16. Tarekegn M, Getachew K, Kenea G. Experimental investigation of concrete characteristics strength with partial replacement of cement by hybrid coffee husk and sugarcane bagasse ash. Adv Mater Sci Eng. 2022;2022:5363766. https://doi.org/10.1155/2022/5363766.
17. Rebari M, Agrawal Y, Gupta T, Sharma R. Mechanical properties of sustainable concrete containing sugarcane bagasse ash: a review. Int Res J Eng Technol. 2020;7:150–63.
18. Praveenkumar S, Sankarasubramanian G. Mechanical and durability properties of bagasse ash-blended high-performance concrete. SN Appl Sci. 2019;1:1–7. https://doi.org/10.1007/s42452-019-1711-x.
19. Khawaja SA, Javed U, Zafar T, Riaz M, Zafar MS, Khan MK. Eco-friendly incorporation of sugarcane bagasse ash as partial replacement of sand in foam concrete. Clean Eng Technol. 2021;4: 100164. https://doi.org/10.1016/j.clet.2021.100164.
20. Sousa LN, Rodrigues CDS. Feasibility of Using Sugar Cane Bagasse Ash in Partial Replacement of Portland Cement Clinker. Buildings. 2023;13:843. https://doi.org/10.3390/buildings13040843.
21. Mangi SA, Dildar AM, Hemu K, Zahid H, Touqeer AR, Mohd HWI. Strength performance of mortar prepared with SCBA and RHA as supplementary cementitious materials at elevated temperatures. Eng Technol Appl Sci Res. 2024;14:16193–7. https://doi.org/10.48084/etasr.7420.
22. Buregyeya A, Nwaubani S, Schmidt W, Kerali AG, Bagampadde U. Pozzolanic and hydration properties of kamafugites and carbonatitic lavas as supplementary cementitious materials in Portland cement. Afr J Sci Technol Innov Dev. 2018;10:845–59. https://doi.org/10.1080/20421338.2018.1527539.
23. Buregyeya A, Ballim Y, Nwaubani S, Kerali AG, Otieno M. Effect of carbonate minerals and calcination of carbonatites and kamafugites on their pozzolanic performance and early age concrete properties. In: Calcined clays for sustainable concrete. RILEM bookseries. Dordrecht: Springer; 2018.
24. Bakera AT, Alexander MG. Properties of western cape concretes with metakaolin. EDP Sci. 2018;199:1–14. https://doi.org/10.1051/matecconf/201819911011.

25. Mousavinezhad S, Newtson CM. Replacing fly ash with a natural pozzolan in normal strength concrete and ultra-high performance concrete. EDP Sci. 2024;396:1–13. https://doi.org/10.1051/matecconf/202439602007.
26. Ranger M, Tange M, Lindgård J, Antonio R. Laboratory and field investigations of alkali-silica reaction prevention by supplementary cementitious materials: influence of the free alkali loading. Constr Build Mater. 2024;442: 137599. https://doi.org/10.1016/j.conbuildmat.2024.137599.
27. De Souza DJ, Sanchez LFM. Evaluating the efficiency of SCMs to avoid or mitigate ASR-induced expansion and deterioration through a multi-level assessment. Cem Concr Res. 2023;173: 107262. https://doi.org/10.1016/j.cemconres.2023.107262.
28. Kannur B, Chore HS. Utilization of sugarcane bagasse ash as cement-replacing materials for concrete pavement: an overview. Innov Infrastruct Solut. 2021;6:184. https://doi.org/10.1007/s41062-021-00539-4.
29. Channa SH, Mangi SA, Bheel N, Soomro FA, Khahro SH. Short-term analysis on the combined use of sugarcane bagasse ash and rice husk ash as supplementary cementitious material in concrete production. Environ Sci Pollut Res. 2022;29:3555–64. https://doi.org/10.1007/s11356-021-15877-0.
30. Xu Q, Ji T, Gao SJ, Yang Z, Wu N. Characteristics and applications of sugar cane bagasse ash waste in cementitious materials. Materials. 2018;12:39. https://doi.org/10.3390/ma12010039.
31. Thomas BS, Yang J, Bahurudeen A, Abdalla JA, Hawileh RA, Hamada HM, Nazar S, Jittin V, Ashish DK. Sugarcane bagasse ash as supplementary cementitious material in concrete—a review. Mater Today Sustain. 2021;15: 100086. https://doi.org/10.1016/j.mtsust.2021.100086.
32. Chen S, Zheng Y, Wu M, Hu J, Xiang W. Thermodynamic analysis of oxy-fuel combustion integrated with the sCO_2 Brayton cycle for combined heat and power production. Energy Convers Manag. 2021;232: 113869. https://doi.org/10.1016/j.enconman.2021.113869.
33. Hassn A, Chiarelli A, Dawson A, Garcia A. Thermal properties of asphalt pavements under dry and wet conditions. Mater Des. 2016;91:432–9. https://doi.org/10.1016/j.matdes.2015.11.116.
34. Hedayati-Dezfooli M, Leong WH. An experimental study of coupled heat and moisture transfer in soils at high temperature conditions for a medium coarse soil. Int J Heat Mass Transf. 2019;137:372–89. https://doi.org/10.1016/j.ijheatmasstransfer.2019.03.131.
35. Radko T, Wajda A, Iluk T, Najser J. Investigation on the correlation between mechanical strength, grain size, and density of fly ash microspheres in the context of refining process. Materials. 2024;17:1–16. https://doi.org/10.3390/ma17143459.
36. Ahmed A. Chemical reactions in pozzolanic concrete. Mod Approach Mater Sci. 2019;1:128–33. https://doi.org/10.32474/mams.2019.01.000120.
37. Choudhary HK, Anupama AV, Kumar R, Panzi ME, Matteppanavar S, Sherikar BN, Sahoo B. Observation of phase transformations in cement during hydration. Constr Build Mater. 2015;101:122–9. https://doi.org/10.1016/j.conbuildmat.2015.10.027.
38. Panzi Mukhokosi E, Mukwaya GW, Enjiku B. Structural and mechanical properties of non-glazed ceramic tiles developed from selected mineral deposits in Uganda. Nano-Horizons. 2023;2:1–14. https://doi.org/10.25159/nanohorizons/13816.
39. Kannur B, Chore HS. Assessing semiflowable self-consolidating concrete with sugarcane bagasse ash for application in rigid pavement. J Mater Civ Eng. 2023;35:16355. https://doi.org/10.1061/jmcee7.mteng-16355.
40. Zuschlag P, Machner A, Hemstad P, Kjellsen KO, Zajac M, Ben Haha M, Danner T, Harald J, Klaartje DW, Mette RG. Hydration of composite cements containing novel SCMs. Nord Concr Res. 2024;5:77–97. https://doi.org/10.2478/ncr-2024-0003.
41. Black L, Brooker A. SEM-SCA: combined SEM—Raman spectrometer for analysis of OPC clinker. Adv Appl Ceram. 2007;106:327–34. https://doi.org/10.1179/174367607X228052.
42. Stutzman P, Leigh S. Phase composition analysis of the NIST reference clinkers by optical microscopy and x-ray powder diffraction reference clinkers by optical diffraction. NIST Tech Note. 2002;1441:44.
43. Bheel N, Ali MOA, Tafsirojjaman, Khahro SH, Keerio MA. Experimental study on fresh, mechanical properties and embodied carbon of concrete blended with sugarcane bagasse ash, metakaolin, and millet husk ash as ternary cementitious material. Environ Sci Pollut Res. 2022; 29:5224–5239. https://doi.org/10.1007/s11356-021-15954-4.
44. J. Payá, J. Monzó, M. V. Borrachero, M.M. Tashima, L. Soriano. Waste and supplementary cementitious materials in concrete. In: Characterisation, properties and applications. Woodhead publishing series in civil and structural engineering. 2018. p. 559–598. https://doi.org/10.1016/B978-0-08-102156-9.00017-1.
45. Khaskhanova LM, Razumova SN, Serebrov DM, Gureva ZA, Vetchinkin AV, Rebrii AV, Said OMHB. Scanning electron microscopy. J Int Dent Med Res. 2022;15:107–10. https://doi.org/10.21273/hortsci.9.5.414.
46. ASTM. ASTM C618–12a: standard specification for coal fly ash and raw or calcined natural pozzolan for use. 2014. p. 1–5. https://doi.org/10.1520/C0618.
47. Bahurudeen A, Wani K, Basit MA, Santhanam M. Assesment of pozzolanic performance of sugarcane bagasse ash. J Mater Civ Eng. 2016;28:1–11. https://doi.org/10.1061/(asce)mt.1943-5533.0001361.
48. Sahin DD, Cavusoglu I, Yilmaz AO. Evaluation of pozzolanic activity of two different types of C and F fly ashes with fineness factor. J Min Environ. 2023;14:435–48. https://doi.org/10.22044/jme.2023.12795.2324.
49. Mehta PK, Monteiro PJM. Concrete: microstructure, properties and materials. 3rd ed. New York: McGraw-Hill; 2006.
50. Yusuf IT, Jimoh YA, Salami WA. An appropriate relationship between flexural strength and compressive strength of palm kernel shell conc rete. Alex Eng J. 2016;55:1553–62. https://doi.org/10.1016/j.aej.2016.04.008.
51. Rossignolo JA, Rodrigues MS, Frias M, Santos SF, Junior HS. Improved interfacial transition zone between aggregate-cementitious matrix by addition sugarcane industrial ash. Cem Concr Compos. 2017;80:157–67. https://doi.org/10.1016/j.cemconcomp.2017.03.011.